

Flexibility of β -sheets: Principal-component analysis of database protein structures

Eldon G. Emberly¹, Ranjan Mukhopadhyay², Chao Tang², and Ned S. Wingreen^{2,*}

¹*Center for Studies in Physics and Biology, The Rockefeller University,
1280 York Ave., New York, NY 10021*

²*NEC Laboratories America, Inc.,
4 Independence Way,
Princeton, NJ 08540*

* *corresponding author: email: wingreen@nec-labs.com*

P: (609) 951-2654 F: (609) 951-2496

(November 1, 2018)

keywords: beta-sheet, flexibility, principal-component analysis, secondary structure

Abstract

Protein folds are built primarily from the packing together of two types of structures: α -helices and β -sheets. Neither structure is rigid, and the flexibility of helices and sheets is often important in determining the final fold (*e.g.*, coiled coils and β -barrels). Recent work has quantified the flexibility of α -helices using a principal-component analysis (PCA) of database helical structures (Emberly, 2003). Here, we extend the analysis to β -sheet flexibility using PCA on a database of β -sheet structures. For sheets of varying dimension and geometry, we find two dominant modes of flexibility: twist and bend. The distributions of amplitudes for these modes are found to be Gaussian and independent, suggesting that the PCA twist and bend modes can be identified as the soft elastic normal modes of sheets. We consider the scaling of mode eigenvalues with sheet size and find that parallel β -sheets are more rigid than anti-parallel sheets over the entire range studied. Lastly, we discuss the application of our PCA results to modeling and design of β -sheet proteins.

I. INTRODUCTION

Most protein folds can be viewed as compact packings of a fixed set of secondary-structural elements^{1,2}: α -helices and β -sheets. It can be reasoned that the formation of these elements greatly simplifies the folding free-energy landscape by reducing the number of degrees of freedom. As a first approximation, helices and sheets can be considered as rigid objects, possessing only six degrees of freedom each (three translations and three rotations). However, most helices and sheets display some amount of bending in a protein's final fold. Understanding to what extent these elements are flexible, and which are their dominant

degrees of freedom, will help to further our understanding of how proteins fold, and even how they function.

A number of studies have extracted the flexible motions of biological molecules using normal-mode and principal-component analysis (PCA).³⁻¹¹ A recent PCA analysis of α -helices from a structural database revealed three “soft” modes: two degenerate bend modes and a twist mode.¹¹ For all but the longest helices, these three modes were sufficient to describe the deformations observed in real structures.

Arguably, a quantitative understanding of flexibility is more important for β -sheets than for α -helices. In natural structures, sheets display a variety of highly distorted and bent shapes, *e.g.* β -barrels and twisted sheets, while helices are generally much less distorted. What are the dominant collective motions of β -sheets and how do they depend on the sheet’s size? Also how does sheet geometry affect the flexibility of a sheet? The “geometry” of a β -sheet is the amino-terminal to carboxyl-terminal orientation of the various strands making up the sheet. Most sheets fall into one of two geometries - parallel, where all the strands are oriented in the same direction, or anti-parallel, where strands alternate direction. The geometry dictates the hydrogen-bonding pattern within the sheet and hence plays a role in determining the sheet’s flexibility.

Here, we report a principal-component analysis of the flexibility of parallel and anti-parallel β -sheets from the Protein Data Bank. The sheets considered range in size from 3 to 6 strands, with 3 to 6 residues per strand. For both parallel and anti-parallel sheets, we find two dominant modes of flexibility: twisting about an in-plane axis that is perpendicular to the strand orientation, and bending of this same axis. The distributions of amplitudes for these two modes are independent Gaussians. Thus, the principal-component modes can be interpreted as dynamical normal modes of an elastic object. Motivated by this interpretation, we consider the scaling of mode eigenvalues (variances of amplitudes) with sheet size, and compare to predictions of a simple elastic model. For all sizes considered, parallel sheets are more rigid than anti-parallel sheets.

Recently, β -sheet structures have been characterized in detail by Ho and Curmi.¹² This database study focused on average properties of sheets, including twist, shear, and hydrogen bonding. In contrast, our PCA analysis of β -sheets provides a characterization of the *flexibility* of sheets about their average structures. Possible applications of the results reported here on sheet flexibility include improved parameterization of force-field models and inclusion of sheet elastic energies in β -protein design.

II. RESULTS

A. Principal-component analysis of database β -sheets

The first step in analyzing the flexibility of β -sheets was to obtain a representative set of structures. Following the procedure described in Methods, we were able to create a database of 3516 representative β -sheets of different geometries. In Fig. 1 we show the distribution of geometries (parallel, anti-parallel, etc.) for sheets consisting of at least 6 strands. For sheets that have more than 6 strands, we consider all the 6 stranded sub-sheets (*e.g.* an 8 stranded sheet would contain three 6 strand sheets). The strand directions are labeled ‘u’ for up and

‘d’ for down, as if the sheet were lying flat on the page. By convention, the first strand is always oriented in the up direction, *i.e.* with the amino-terminal at the bottom of the page and the carboxyl-terminal at the top of the page. Since each of the two outermost strands of a sheet can be equally well regarded as the first strand, the distribution of geometries in Fig. 1 includes every sheet twice. We find that the distribution of geometries is highly non-uniform, with the most frequent types being parallel (uuuuuu) and anti-parallel (ududud). Because other geometries occur so infrequently, we focus the rest of the analysis on parallel and anti-parallel sheets.

Sets of defect-free β -sheets of a given class were extracted from the 3516 representative β -sheets. Sheets are of the same class if they have the same size, S strands each of length L , geometry, and pleatedness or corrugation (see Methods). To quantify flexibility, we performed a structural principal-component analysis (PCA) for each class of sheets, to identify the dominant collective fluctuations around the mean structure. To implement the PCA, we first computed the mean structure for each class of sheets via an iterative procedure. Starting with a randomly chosen sheet of the desired class, we aligned to it all other sheets of the same class. To align two sheets, we minimized the coordinate root mean square (crms) distance between their corresponding C_α atoms. A mean structure was then obtained by averaging the position of each C_α atom over all the aligned structures. This procedure was iterated, each time using the new mean structure as the basis for alignment, until the mean structure converged to within 10^{-4} Å/residue. An example of a subset of structures aligned to the converged mean structure is shown in Fig. 2. For anti-parallel sheets we find that the average structure conforms to the sheared structure discussed in Ho and Curmi¹². They also showed that parallel sheets are less sheared and we find this to be the case for our average parallel sheets.

The second step in the principal-component analysis was to compute the structural covariance matrix for each class of sheet. A covariance matrix measures the correlation of the variation from the mean for each pair of coordinates. In our case, there were $3SL$ coordinates – 3 spatial directions for each of $S \times L$ C_α atoms. Consequently, the covariance matrix was a $3SL \times 3SL$ matrix, with elements i, j defined as

$$C_{i,j} = \frac{1}{N-1} \sum_{m=1}^N (x_{mi} - \langle x_i \rangle)(x_{mj} - \langle x_j \rangle), \quad (1)$$

where N is the number of sheets in the given class, x_{mi} is the i^{th} coordinate of the m^{th} structure, and $\langle x_i \rangle$ is the i^{th} coordinate of the mean structure.

To complete the principal-component analysis, we computed the eigenvalues $\{\lambda_q\}$ and eigenvectors $\{\vec{v}_q\}$ of the covariance matrix for each class of sheets (available as Supplementary Material). The largest eigenvalues and corresponding eigenvectors represent the directions for which the data has the largest variance. These directions are the “soft” modes of the sheets, *i.e.* those collective deformations that appear with largest amplitude in the data set. Figure 3 shows the top 10 eigenvalues for anti-parallel sheets of size $S = 4$ and $L = 5$, as shown in Fig. 2. Each eigenvalue is given in units of Å² and measures the variance of the distribution for a particular mode. Two dominant eigenvalues are evident in Fig. 3. The first mode is primarily a twist of the sheet about the in-plane axis perpendicular to the strand orientation (Fig. 4(a)). The second mode is primarily a bend of the sheet along the same axis (Fig. 4(b)).

For all the classes of sheets considered, we found two dominant soft modes. The eigenvalues (*i.e.* variances) of these modes are shown for different sheet sizes and geometries in Figs. 5 and 6. Figure 5 shows the scaling of the eigenvalues with the number of strands S for sheets of fixed strand length. The bend-mode eigenvalues increase approximately as S^4 , while the twist-mode eigenvalues increase more slowly with S (fits to S^4 for the anti-parallel bend modes are shown). As a result of this difference in scaling, the eigenvalues for the twist and bend modes cross with increasing number of strands. For five or more strands, the eigenvalue for the bend mode becomes the larger, implying greater deformations of the sheet by bending compared to twisting. Figure 6 shows the scaling of the eigenvalues with the strand length L for sheets with a fixed number of strands. The eigenvalues generally increase with strand length, scaling roughly as L or L^2 . The scaling behavior expected for pure bend and twist modes is discussed in the next section.

A feature that emerges from the scaling graphs is that the twist-mode and bend-mode eigenvalues are almost always larger for anti-parallel sheets than for parallel sheets. Since these two modes dominate deviations from the mean structure, this implies that total deformations are typically larger for anti-parallel sheets than for parallel sheets.

Next, we consider the actual distributions of amplitudes for the dominant twist and bend modes. The displacement of a given sheet from the mean structure, $\delta\vec{x} = \vec{x} - \langle\vec{x}\rangle$, can be expanded in terms of the PCA eigenvectors as $\delta\vec{x} = \sum_q a_q \vec{v}_q$. The amplitude a_q is given by the projection of the displacement vector $\delta\vec{x}$ onto mode q . Figures 7(a and b) show the distributions of projections onto twist and bend for the 1454 anti-parallel sheets with $S = 4$ and $L = 5$ (cf. Fig. 2). The two distributions can be fit well by Gaussians, with the variances of the Gaussians, 9.6985 \AA^2 for twist and 4.3655 \AA^2 for bend, close to the exact variances given by the mode eigenvalues, 7.7876 \AA^2 for bend and 4.0044 \AA^2 for twist. By construction, all PCA modes are uncorrelated to lowest order, *i.e.* $\langle a_q a_{q'} \rangle = 0$, for $q \neq q'$. To look for possible higher-order correlations, we made a scatter plot of the amplitudes for the two dominant modes, as shown in Fig. 7(c). The distributions of points is roughly ellipsoidal, indicating that there are no strong higher-order correlations between modes. Similar independent Gaussian distributions were obtained for all classes of sheets for which PCA analysis was performed.

The Gaussian distributions of mode amplitudes and the lack of higher-order correlations between modes suggest that the PCA modes can be interpreted as the *dynamical* modes of a β -sheet. This is consistent with previous results for α -helices showing the near identity between PCA modes obtained from static structures and the elastic normal modes of a model helix.¹¹ For small amplitude motions, elastic normal modes at equilibrium have independent Gaussian distributions $P(a_q)$ determined by Boltzmann weights

$$P(a_q) \sim e^{-E(a_q)/k_B T} \sim e^{-c_q a_q^2 / 2k_B T}, \quad (2)$$

where $E(a_q) = c_q a_q^2 / 2$ is the deformation energy as a function of the mode amplitude a_q , and c_q is the spring constant for the mode. The “soft” modes have the smallest spring constants, and therefore the broadest spread of amplitudes.

B. Scaling of the PCA modes

Guided by the interpretation of the PCA modes as the elastic normal modes of a sheet, we consider the scaling with sheet size of the mode eigenvalues. Let us first consider the dominant bend mode, as shown in Fig. 4(b). For a uniform bend of the in-plane axis perpendicular to the strand orientation, the displacement of the strand at position x along this axis goes as $\delta z \simeq x^2/R$, where R is the radius of curvature. The bending eigenvalue is given by $\lambda_{\text{bend}} = \langle |\delta \vec{z} \cdot \vec{v}|^2 \rangle$ where \vec{v} is the normalized eigenvector. It follows that

$$\lambda_{\text{bend}} \sim LS^5 \langle \frac{1}{R^2} \rangle, \quad (3)$$

where L is the strand length and S is the number of strands. At thermal equilibrium, each normal mode has $k_B T/2$ of potential energy. For the bend mode, this energy would be put into curvature of the axis:

$$\frac{1}{2}k_B T = \frac{1}{2}\kappa LS \langle \frac{1}{R^2} \rangle, \quad (4)$$

where κ is the bend stiffness per unit length, indicating

$$\lambda_{\text{bend}} \sim \frac{k_b T}{\kappa} S^4. \quad (5)$$

Thus the eigenvalue for a pure bend mode would scale as S^4 and would be independent of L . In Fig. 5, the predicted S^4 scaling of the bend-mode eigenvalue is seen for both parallel and anti-parallel β -sheets. In Fig. 6, however, we observe a significant increase of the eigenvalue with L , which is not predicted. The reason for the increase of the bend-mode eigenvalue with strand length L is likely to be the significant bending of individual strands associated with this mode, which would contribute a term to λ_{bend} that scales as L^4 .

For the twist mode, as shown in Fig. 4(a), we assume that each strand rotates by an angle $\delta\theta$ with respect to its neighboring strand. This corresponds to a uniform twist of the sheet about the in-plane axis perpendicular to the strand orientation. The displacement of a C_α atom on the strand at x along this axis, and at a distance l from this axis, is $\delta z \simeq l(x/d)\delta\theta$, where d is the distance between neighboring strands. It is straightforward to show that eigenvalue for the twist mode goes as

$$\lambda_{\text{twist}} \sim \langle \delta\theta^2 \rangle L^3 S^3 \quad (6)$$

At thermodynamic equilibrium, using $k_B T = c \langle \delta\theta^2 \rangle LS$, where c is a twist stiffness per unit length, we find $\lambda_{\text{twist}} \sim L^2 S^2$. As shown in Fig. 6, the twist-mode eigenvalue does scale as L^2 as predicted, at least for sheets of up to $S = 5$ strands. As seen in Fig. 5, however, the scaling of the twist-mode eigenvalue with strand number is much weaker than the predicted S^2 , for all strand lengths.

III. DISCUSSION

Our principal-component analysis of β -sheets indicates that sheets in proteins are formed primarily in two ways, by twisting and bending. The amplitudes of these modes

were found to have independent Gaussian distributions, suggesting that twist and bend are the “soft” elastic modes of sheets. The interpretation of the PCA twist and bend modes as elastic modes of sheets is consistent with previous PCA results on α -helices. For helices, the dominant modes found by PCA were shown to be indistinguishable from the soft elastic modes of a model helix.¹¹

In this light, the generally larger twist and bend deformations found for anti-parallel sheets compared to parallel sheets suggests that anti-parallel sheets have softer elastic spring constants. This could arise from boundary effects imposed by the differences in connectivity. Anti-parallel sheets tend to be connected by short loops which allows the sheet to be easily bent. In contrast, parallel sheets have more complex connectivity (long loops) which could impinge on their ability to deform. The stiffness may also arise due to slight differences in the hydrogen bonding pattern between parallel and sheared anti-parallel sheets¹². It will be interesting to see if physical modeling can capture the apparent differences in elasticity between the two types of sheets.

While the PCA modes of all β -sheets studied had the characteristics of elastic normal modes (*i.e.*, independent Gaussian distributions of amplitudes) significant deviations from simple scaling with sheet size were observed. These deviations can probably be attributed to two main causes. First, the actual soft modes are not the pure twist and bend modes of rigid strands as assumed in the scaling analysis. Significant deformations do occur within individual strands - the bend mode also contains bending along the strands which would contribute to the scaling of its eigenvalue with strand length L . Second, β -sheets, as quasi-two-dimensional objects, are subject to strong boundary effects. For example, the constraint of global connectivity of the sheets and the need to form backbone hydrogen bonds to the outer strands are likely to introduce size-dependent effects beyond the simple scaling analysis. In contrast, the nearly ideal scaling of the dominant modes of α -helices probably reflects the much weaker effect of boundaries on quasi-one-dimensional objects.¹¹

Our PCA results provide a set of scaling behaviors and structural properties that can be used to test and refine energetic models of β -sheets. We have found that a simple spring model, similar to one that was able to capture the normal modes of helices¹¹, did not describe well the scaling properties of sheets. This suggests that the energetics governing β -sheet flexibility is more complex than in helices. More detailed force fields are required and these will help to further clarify the microscopic interactions governing β -sheet structure and flexibility.

Another possible application of the PCA results is to protein design. A recent design scheme focussed on the packing of a fixed set of structural elements to explore the space of potential novel folds¹³. In that work, only rigid helices were considered for the structural building blocks. Because of the greater flexibility of sheets compared to helices, extending the packing scheme to sheets will require including energies of elastic deformation. The soft modes of sheets can be easily incorporated into the design of low-energy backbone structures using the elastic energies $E(a_q) = c_q a_q^2 / 2$. Since we found only two dominant modes for sheets, elasticity can be added to the packing scheme with only two extra degrees of freedom per sheet. The soft modes could also be incorporated into models that analyze how a specific protein’s structure is changed when the sequence is mutated or redesigned. Inclusion of soft modes may prove particularly useful in redesign of binding sites, which is currently limited to the rigid-backbone approximation¹⁴.

In summary, this work has used database protein structures to reveal the flexible motions of β -sheets. The effective spring constants and eigenvectors for the sheets studied, as well as the mean structure coordinates, are available as Supplementary Material.

IV. METHODS

We compiled a set of β -sheet structures from 2860 representative protein folds in the FSSP database¹⁵. The representative structures in the FSSP are the structurally distinct folds that result from doing an all-against-all structure clustering of protein folds that have less than 25% sequence identity. Thus the set is designed to minimize fold redundancy. Making use of the structural annotations in the PDB files for the representative set, we extracted the β -sheets from each fold. Only sheets within a certain size range were considered: sheets had to have at least 3 strands and no more than 25, with between 3 and 15 residues per strand. Using these criteria we were able to extract 3516 representative β -sheets.

Many of the sheets in this representative set were found to have defects. A defect occurs when there is a gap in the hydrogen-bonding pattern, or the strands are of different lengths and one overhangs the other. These two types of defects are schematically illustrated in Fig. 8. We wished to eliminate sheets with defects before performing a principal-component analysis of flexibility. To systematically identify defects, we developed a procedure for finding the optimal pairing of C_α atoms on adjacent strands. A defect is indicated when a C_α atom is left unpaired. To find the optimal pairing, we computed a distance matrix $d_{i,j}$ for each pair of neighboring strands,

$$d_{i,j} = |\vec{r}_i - \vec{r}_j| \quad (7)$$

where \vec{r}_i is the position of the i th C_α atom on the first strand and \vec{r}_j is the position of the j th C_α atom on the second strand. The two strands could be of different lengths. We defined the optimal pairing $i \leftrightarrow j$ between strands to be the one which minimized

$$D = 6\text{\AA}N_{\text{gaps}} + \sum_{\text{pairs } i,j} d_{i,j} \quad (8)$$

where the last term represents a penalty of $+6\text{\AA}$ for each gap. A gap occurs when a C_α atom on one strand is not paired. In practice, we found that a gap penalty of 6\AA identified gaps in good agreement with a visual inspection of the sheets. To efficiently find the optimal pairing, *i.e.* the one which minimizes D , we employed the Needleman-Wunsch method¹⁶ for global sequence alignment. We applied the alignment procedure for each neighboring pair of strands in the sheet (strands in the sheet tend to be annotated in the order they occur in the sheet, hence the need to only align neighbors). This gave us the optimal alignment of all the strands in the sheet, and allowed us to identify sheet defects.

After performing the pairwise alignment of all the strands making up a sheet we then extracted sheets of a fixed size, *e.g.* S strands each of length L . This is illustrated in Fig. 8(a). We scanned the aligned sheet using a window of the specified dimension. If the window spanned a region that did not contain a gap, the positions of the C_α atoms were recorded to a file. For each extracted sheet, we also recorded the sheet geometry, *i.e.*

the relative amino-terminal to carboxyl-terminal directions of all the strands in the sheet. The direction of the first strand was defined to be up to simplify the recording of sheet geometries. The choice of which of the two outermost strands to call the first strand was arbitrary, and this was compensated for later. Another quantity recorded for each sheet was its “pleatedness”. A β -sheet is corrugated - it has alternating ridges and valleys. If the first row of atoms from the strands making up a sheet comprise a “ridge” we consider the sheet to have positive pleatedness. If the first row of atoms comprise a “valley” we consider the sheet to have negative pleatedness. The two types of pleatedness are shown in Fig. 8(b). We consider sheets of the same size, geometry, and pleatedness to constitute a “class”. Only sheets of the same class are aligned for subsequent principal-component analysis (see Results).

We note that each extracted ungapped sheet in fact generates two sheets because either of the two outermost strands could be called the “first”. Having arbitrarily chosen a first strand and called its direction up, there are two possible symmetry operations to obtain the second sheet. If the last strand is also up, we flip the sheet (this causes the pleatedness to change sign). If on the other hand the last strand is oriented down, we perform a clockwise rotation of the sheet by 180° . These symmetry operations effectively double our database of sheet structures.

REFERENCES

- ¹ Richardson JS. The anatomy and taxonomy of protein structure. *Advan. Protein Chem* 1981;**34**:167-339.
- ² Chothia C, Levitt M, Richardson D. Structure of proteins: packing of α -helices and pleated sheets. *Proc. Natl. Acad. Sci. USA* 1977;**74**:4130-4134.
- ³ Olson WK, Gorin AA, Lu X-J, Hock LM, Zhurkin VB. DNA sequence-dependent deformability deduced from protein-DNA crystal complexes. *Proc. Nat. Acad. Sci. USA* 1998;**95**:11163-11168.
- ⁴ Kidera A, Go N. Refinement of protein dynamic structure: normal mode refinement. *Proc. Natl. Acad. Sci. USA* 1990;**87**:3718-3722.
- ⁵ Diamond R. On the use of normal modes in thermal parameter refinement: theory and application to the bovine pancreatic trypsin inhibitor. *Acta Crystallogr. A* 1990;**46**:425-435.
- ⁶ Faure P, Micu A, Perahia D, Doucet J, Smith JC, Benoit JP. Correlated intramolecular motions and diffuse X-ray scattering in lysozyme. *Nat. Struct. Biol.* 1994;**1**:124-128.
- ⁷ Tirion MM. Large amplitude elastic motions in proteins from a single-parameter, atomic analysis. *Phys. Rev. Lett.* 1996;**77**:1905-1908.
- ⁸ Haliloulu T, Bahar I, Erman B. Gaussian dynamics of folded proteins. *Phys. Rev. Lett.* 1997;**79**:3090-3093.
- ⁹ Krebs WG, Alexandrov V, Wilson CA, Echols N, Yu H, Gerstein M. Normal mode analysis of macromolecular motions in a database framework: Developing mode concentration as a useful classifying statistic. *Proteins* 2002;**48**:682-695.
- ¹⁰ Travers AA. DNA bending and nucleosome positioning. *Trends Biochem. Sci.* 1987;**12**:108-112.
- ¹¹ Emberly EG, Mukhopadhyay R, Wingreen NS, Tang C. Flexibility of alpha-helices: Results of a statistical analysis of database protein structures. *J. Mol. Biol.* 2003;**327**:229-37.
- ¹² Ho BK, Curmi MG. Twist and shear in β -sheets and β -ribbons. *J. Mol. Biol.* 2002;**317**:291-308.
- ¹³ Emberly EG, Wingreen NS, Tang C. Designability of α -helical proteins. *Proc. Nat. Acad. Sci. USA* 2002;**99**:11163-11168.
- ¹⁴ Looger LL, Dwyer MA, Smith JJ, Hellinga HW. Computational design of receptor and sensor proteins with novel functions. *Nature* 2003; **423**:132-133.
- ¹⁵ Holm L, Sander C. Mapping the protein universe. *Science* 1996;**273**:595-602.
- ¹⁶ For a good review of the Needleman-Wunsch algorithm see "Biological Sequence Analysis", Durbin R, Eddy S, Krogh A, Mitchison G. (2001) Cambridge University Press.

FIGURES

FIG. 1. Distribution of geometries for β -sheets containing at least 6 strands from the set of 3516 representative structures. The strand orientations are labeled with “u” for up and “d” for down, according to amino-terminal to carboxyl-terminal direction. We have fixed the orientation of the first strand to always be up.

FIG. 2. Demonstration set of 10 anti-parallel sheets, of 4 strands each with 5 residues per strand and the same pleatedness (corrugation), all aligned to the average sheet for this class.

FIG. 3. The ten largest eigenvalues from the principal-component analysis of 1454 anti-parallel 4×5 β -sheets, of the class shown in Fig. 2

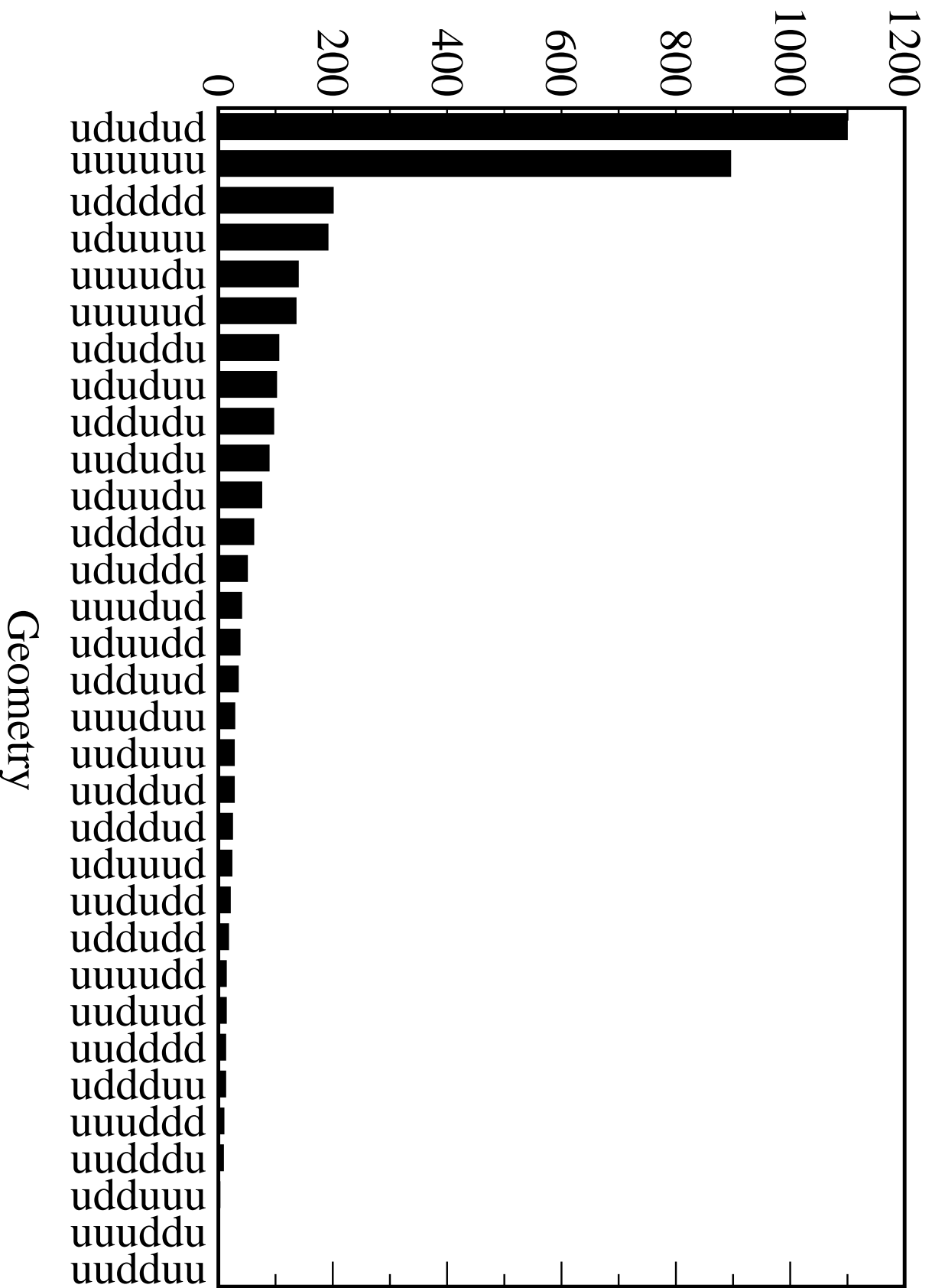
FIG. 4. (a) Exaggerated twist mode of a 6 stranded β -sheet with 5 residues per strand. (b) Exaggerated bend mode of the same sheet. Average structures are shown in gray, deformed structures are shown in red.

FIG. 5. Scaling of the eigenvalues for the bend and twist modes as a function of the number of strands for sheets of fixed strand length. The scalings are shown for both parallel and anti-parallel sheets.

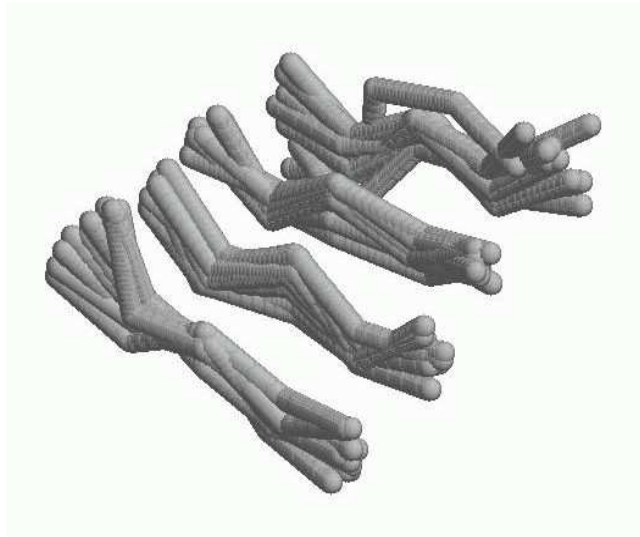
FIG. 6. Scaling of the eigenvalues for the bend and twist modes as a function of strand length for sheets with fixed number of strands. The scalings are shown for both parallel and anti-parallel sheets.

FIG. 7. (a,b) Distribution of the projections of sheet displacement onto the twist and bend modes for 1454 anti-parallel β -sheets each with 4 strands of 5 residues (cf. Fig. 2). Gaussian fits to the distributions are shown by the red curves. (c) Projections onto the subspace spanned by the twist and bend modes for the same 1454 structures.

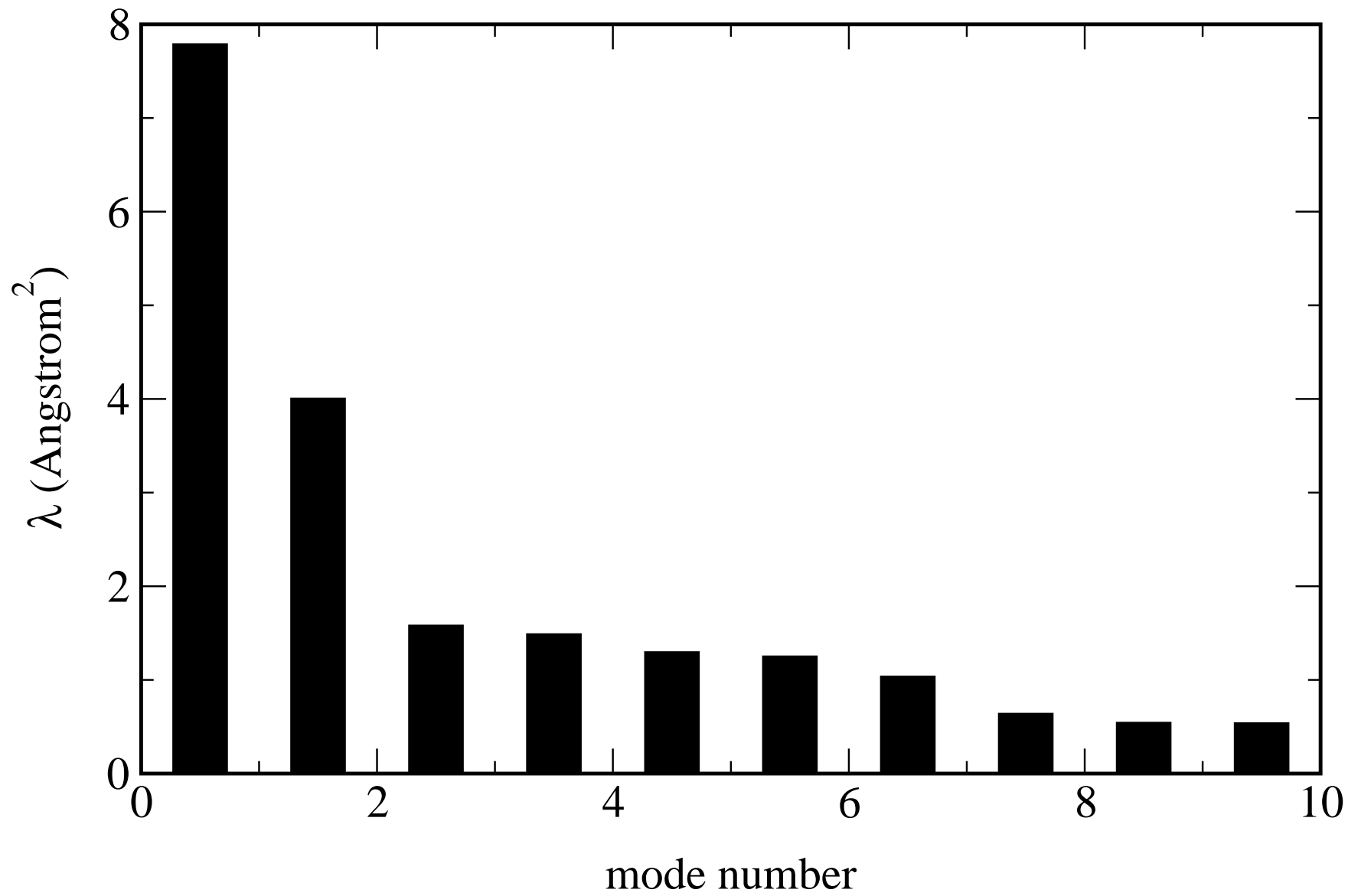
FIG. 8. (a) Schematic of the alignment procedure used to extract β -sheets of a fixed dimension. On the left is sheet that might exist within the database. Backbone C_α atoms are aligned (dashed lines) using a global alignment procedure that allows for gaps. For example, a gap occurs in the bottom strand at the second C_α atom from the left. All ungapped sheets of given dimension (S strands each of length L) are then extracted. (b) The two types of pleatedness. If the first (leftmost) row of atoms forms a ridge, we consider the sheet to have positive pleatedness. If the first row of atoms forms a valley we consider the sheet to have negative pleatedness.



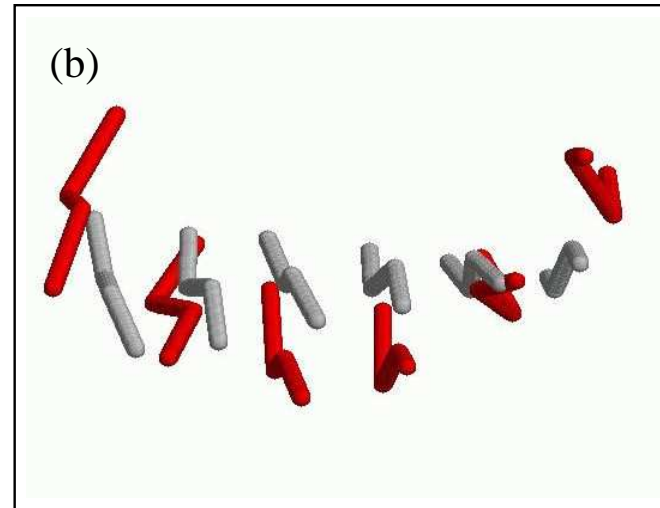
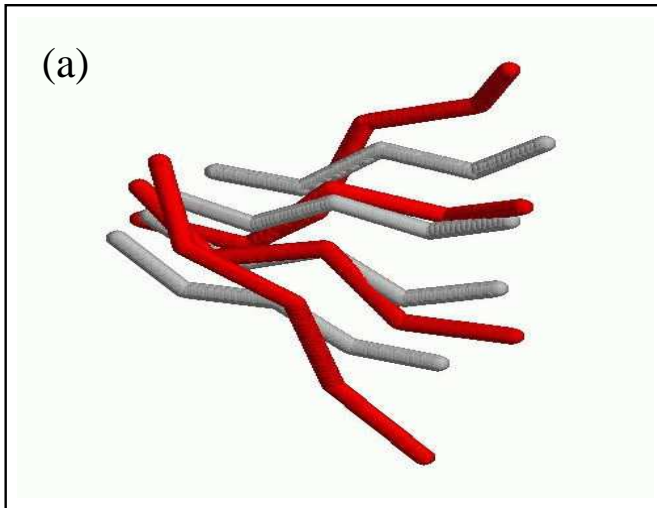
Emberly et al. Fig. 1



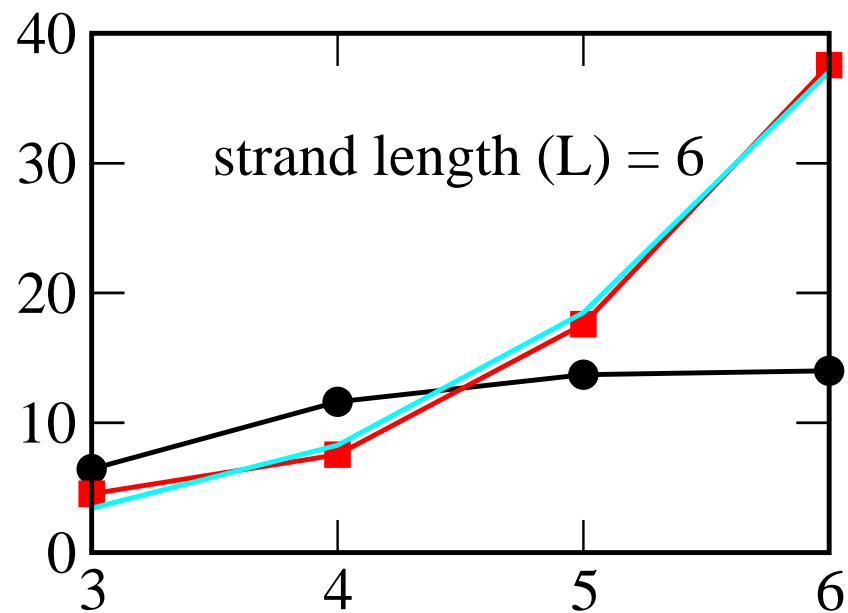
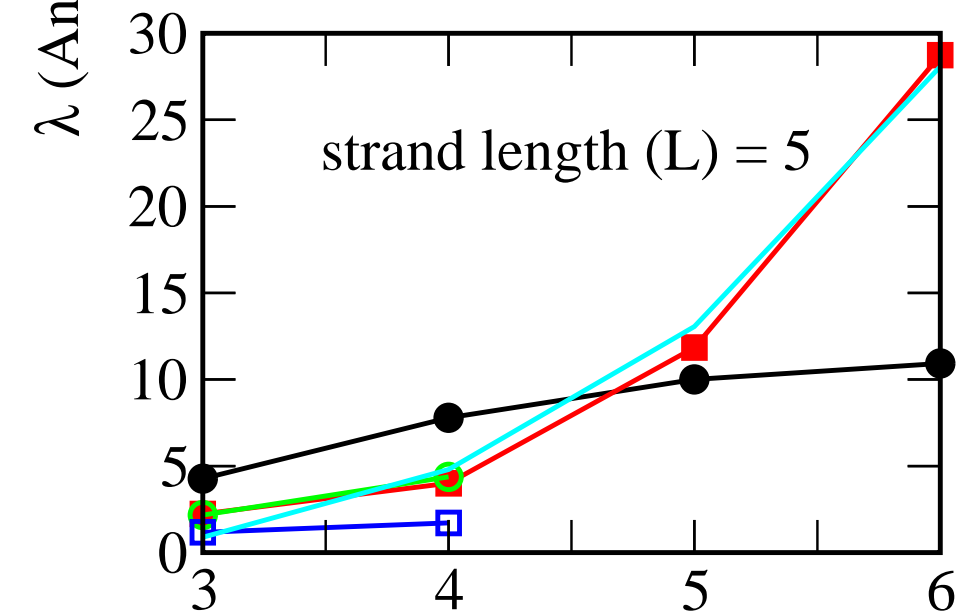
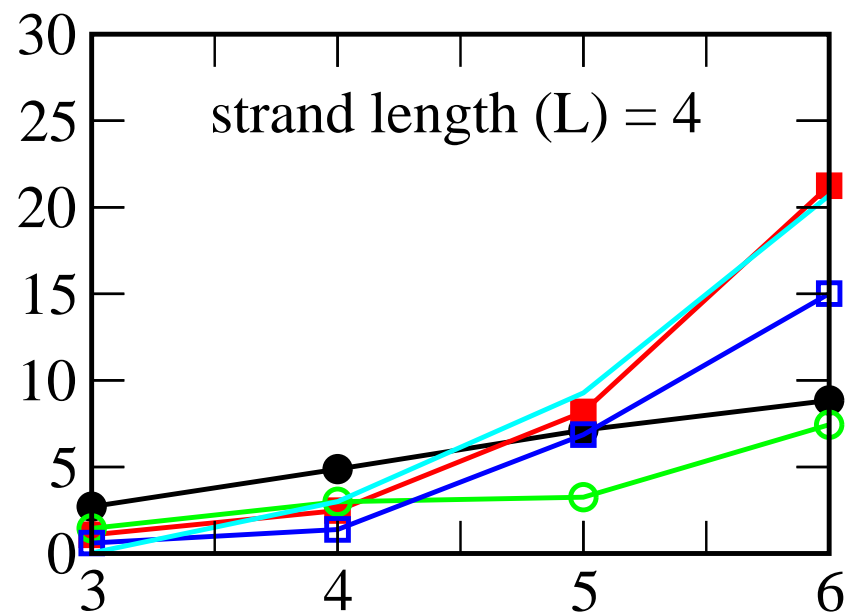
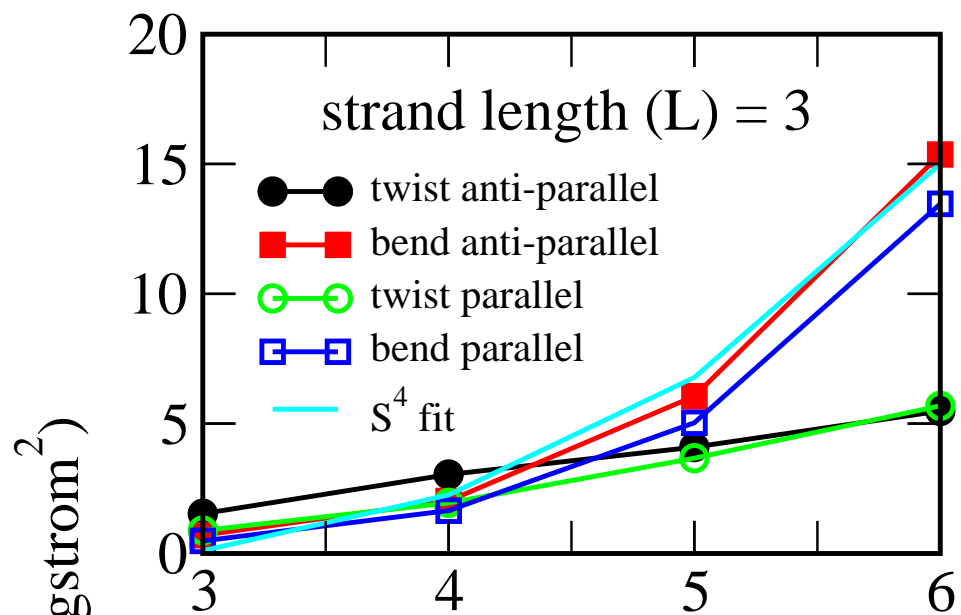
Emberly et al. Fig. 2



Emberly et al. Fig. 3

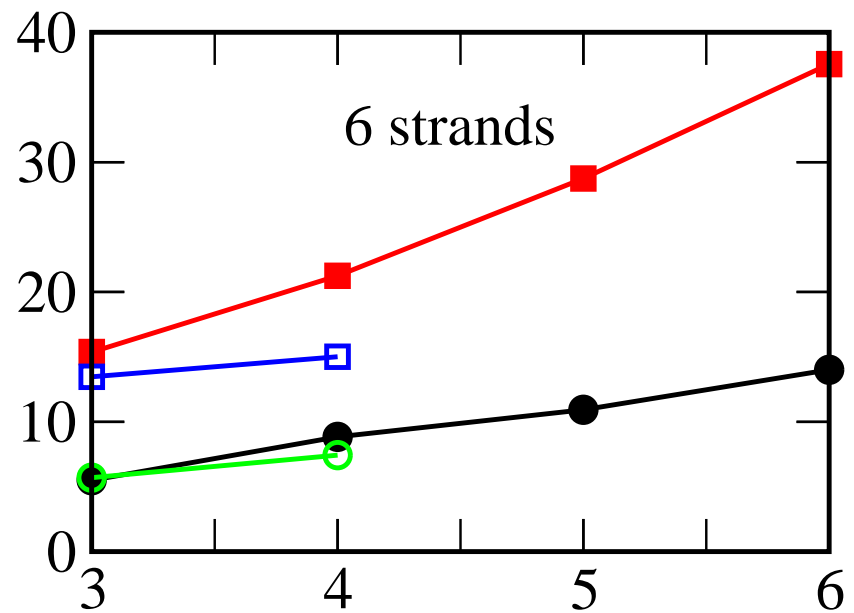
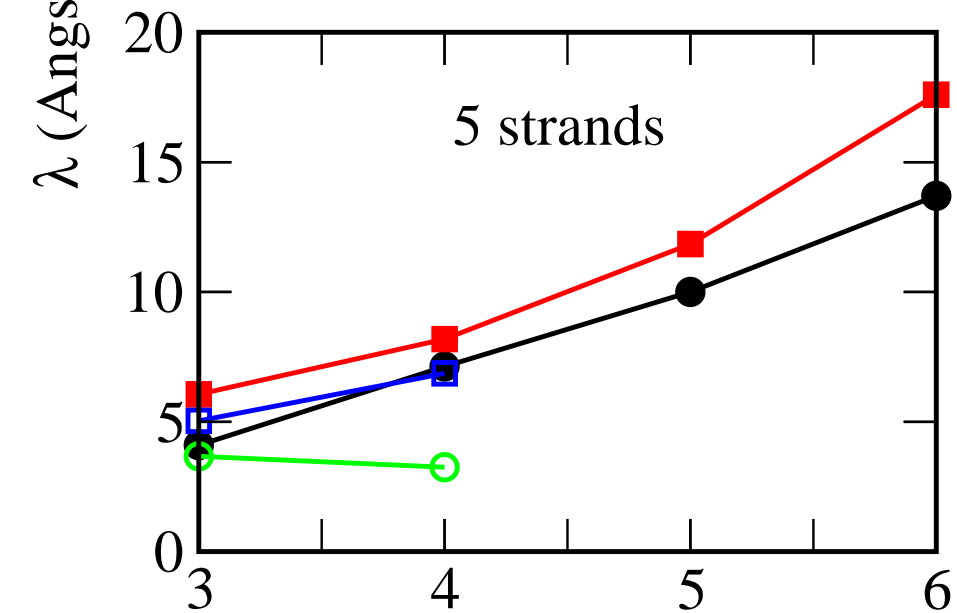
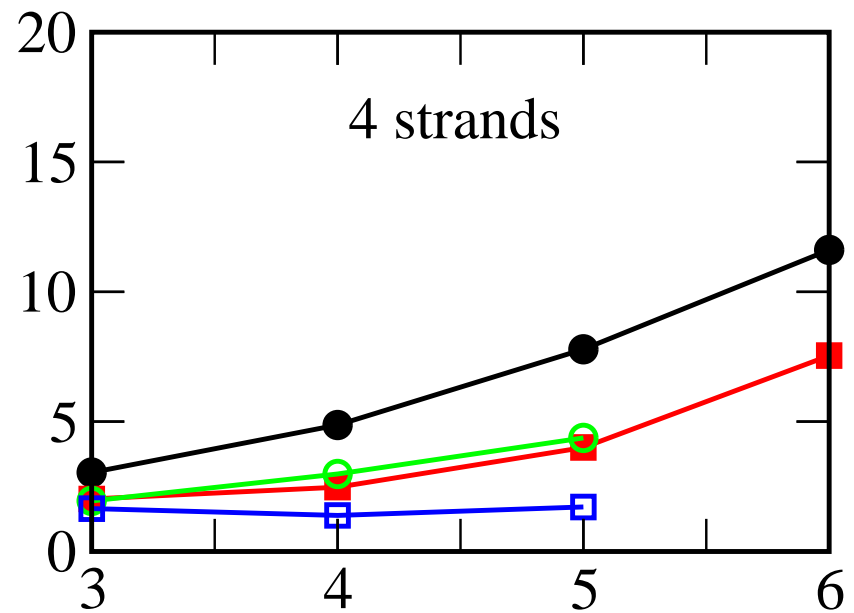
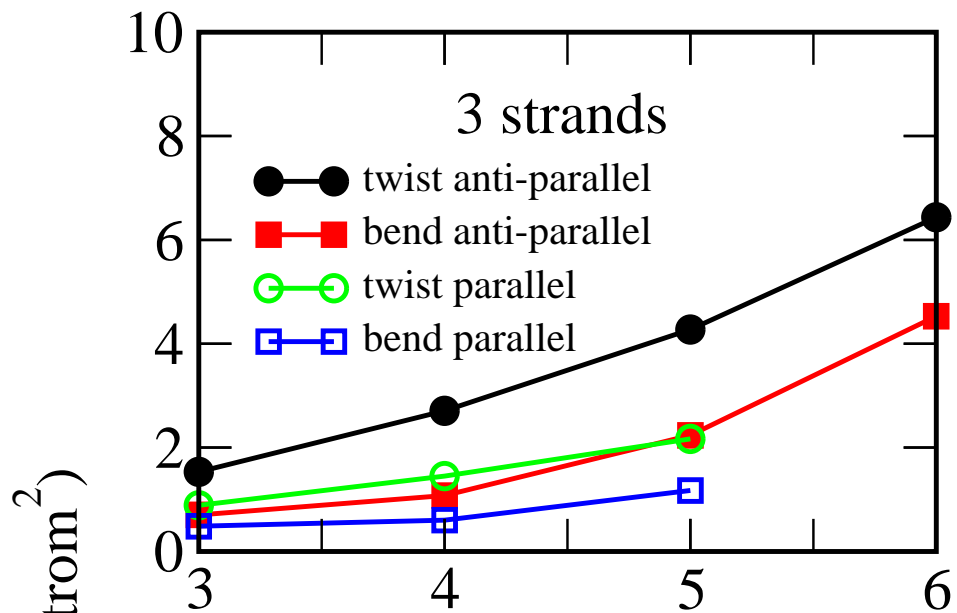


Emberly et al. Fig 4



Number of strands (S)

Number of strands (S)



Length of each strand (L)

Length of each strand (L)

